Modeling of radiation losses in ultrahigh power laser-matter interaction

R. Capdessus,* E. d'Humières, and V. T. Tikhonchuk
University Bordeaux, CNRS, CEA, CELIA, UMR 5107, F-33400 Talence, France
(Received 3 February 2012; published 4 September 2012)

Radiation losses of electrons in ultraintense laser fields constitute a process that can be important for electron and ion acceleration and creation of secondary emissions. The importance of this effect for ion acceleration to high energies is studied as a function of the laser intensity and the target thickness and density. For instance, in the piston regime, radiation losses lead to a reduction of the piston velocity and to less-efficient ion acceleration. Radiation losses have been implemented in the relativistic particle-in-cell code by using a renormalized Lorentz-Abraham-Dirac model.

DOI: 10.1103/PhysRevE.86.036401 PACS number(s): 52.38.Kd, 41.75.Jv, 52.65.Rr, 41.60−m

I. INTRODUCTION

A new generation of laser systems such as planned in the Extreme Light Infrastructure project [1] will produce laser intensities as high as 10^{24} W/cm^2. New physical processes are expected under these conditions such as emission of high-energy photons, the force of radiation reaction acting on electrons, electron-positron pair production, and acceleration of ions to relativistic energies [2]. One of the important applications of ultraintense laser pulses is acceleration of charged particles to extremely high energies. Ion acceleration in the field by an ultrashort and ultraintense laser pulse is one of the most important applications of the presently available compact laser systems with multiterawatt and petawatt power. The process of ion acceleration has been studied in detail in experiments [3] and with multidimensional particle-in-cell (PIC) simulations [4]. In Ref. [5] a plasma produced by an ultrashort and ultraintense laser pulse was proposed as a source of high-energy ions for hadrontherapy in oncology. Recent numerical simulations and theoretical analysis show that at laser intensities exceeding 10^{22} W/cm^2 the ions can be accelerated to relativistic energies under the laser radiation pressure. The importance of taking into account radiation losses under these conditions was demonstrated in Refs. [6,7]. Still, more work needs to be done on the theoretical description of the radiation losses at ultrahigh laser intensity and on their effect on the various laser ion acceleration mechanisms in this regime.

The characteristic spatial scale where the radiation effects become important for relativistic electrons is defined by the Compton length, $\lambda_C = \hbar/m_e c$. If the electric field E acting on the electron is such that it gains a relativistic energy on this length, the radiation processes dominate the interaction. This condition defines the Schwinger field:

$$E_S = m_e^2 c^3/e\hbar,$$

and the dimensionless parameter $\chi_e = E/E_S$. It should be small, $\chi_e \ll 1$, in the electron proper reference frame in the domain where the classical electrodynamics applies. For lasers, the Schwinger field corresponds to the intensity $I_S = \frac{1}{2}\epsilon_0 c E_S^2$ of about 10^{29} W/cm^2. It will be difficult to attain such intensities in the near future. However, radiation effects may become important at lower intensities for relativistic electrons moving towards the laser, as the electric field seen by an electron is enhanced by the factor $\gamma_e(1-\beta_{e\|})$, where $\gamma_e = (1-\beta_e^2)^{-1/2}$ is the electron relativistic factor and $\beta_{e\|}$ is the component of the dimensionless electron velocity parallel to the laser propagation axis. For an electron propagating towards the laser $\beta_{e\|} \approx -1$ and the laser electric field is enhanced by a factor of $\sim 2\,\gamma_e$.

The laser field can be conveniently characterized by the dimensionless parameter $a_L = eE_L/m_e\omega_L c$, which is the ratio of the momentum that an electron gains in the laser field of the frequency ω_L to $m_e c$. Consequently, the Schwinger parameter for the laser reads

$$\chi_e = \gamma_e(1-\beta_{e\|})a_L\hbar\omega_L/m_e c^2.$$

As the electron gains the energy $\gamma_e \sim a_L$ in the laser field, the domain of applicability of the classical electrodynamics is limited by the condition $a_L \ll (m_e c^2/\hbar\omega_L)^{1/2} \simeq 440$ corresponding to laser intensities of about 4×10^{23} W/cm^2.

The classical electron dynamics is described by the Lorentz-Abraham-Dirac (LAD) equation [8]. It accounts for the friction force (also called self-force) acting on an electron due to its own radiation losses. However, the LAD equation contains a third-order time derivative, and it presents nonphysical runaway solutions. It is difficult to apply it even for the description of the dynamics of a single electron [9,10].

A perturbation approach to the solution of the LAD equation was proposed by Landau and Lifshitz (LL) [11] and further detailed by Rohrlich [12]. The LL equation is of the second order in time and it does not contain unphysical solutions, but the radiation reaction may have a noticeable effect on the electron dynamics only in ultrastrong fields. Although for an ultrarelativistic case the radiation reaction force may be comparable to the Lorentz force in the laboratory frame, it remains much smaller than the Lorentz force in the instantaneous frame of the particle as long as the dimensionless Schwinger parameter verifies the condition, $\chi_e \ll 1$ [11,15].

While the radiation reaction force has been applied to the motion of a single particle for a long time, it has only recently been considered in plasma physics. First kinetic simulations of laser-plasma interaction with PIC codes accounting for the radiation force were reported in Refs. [7,13,14]. They demonstrated the role that the radiation reaction plays in the radiation pressure acceleration of ions by high-intensity laser

*capdessus@celia.u-bordeaux1.fr

pulses. During the last five years several models that take into account the effect of radiation losses on the motion of charged particles have been used. One can cite the models by Bell [15], Ford [16], and Sokolov [17]. However, only Sokolov's equations are different from the Landau-Lifshitz model. In their implementation of the radiation reaction force the authors [7] used a new renormalized version of the LAD equation proposed recently in Refs. [17,18] that accounts for the modification of the electron orbit under the action of the self-force. Although still limited by the classical approach condition, $\chi_e < 1$ [19,20], this approach is considered to be more accurate than the LL equation and it is also better suited for numerical implementation in PIC codes. In the present paper, we implemented electron radiation effects in the one-dimensional (1D) relativistic PIC code PICLS [21] and applied it to the study of various regimes of laser ion acceleration at ultrahigh laser intensities. The theoretical approach is developed in Sec. II. The physics of laser plasma interaction is described by the kinetic equations for the electrons, ions, and photons coupled with the large-scale electromagnetic fields described by Maxwell's equations. In particular, the problem of separation of the photons described kinetically and the laser fields described classically is discussed. The numerical implementation of the radiation losses and the self-force in the code PICLS is presented in Sec. III. The numerical scheme is explained, discussed, and compared with several representative results recently published. Finally, the role of electron radiation losses in ion acceleration by strong laser pulses is studied in Sec. IV. Depending on the target density and thickness the radiation reaction may enhance or decrease the energy of ions. The results of the paper are summarized in Sec. V.

II. RADIATION REACTION FORCE

A. Single-electron dynamics

Charged particles in the presence of a strong electromagnetic field emit high-frequency radiation. Its power, $P_r = \frac{2}{3}\frac{q^2}{c^3}\mathbf{w}^2$, is given by the Larmor formula, where q is the particle charge, $\mathbf{w} = (m\gamma)^{-1}[\mathbf{F}_{Le} - (\mathbf{F}_{Le}\cdot\boldsymbol{\beta})\,\boldsymbol{\beta}]$ is the particle acceleration by the Lorentz force

$$\mathbf{F}_{Le} = q\,(\mathbf{E} + \boldsymbol{\beta}\times\mathbf{B})\,, \tag{1}$$

and $\boldsymbol{\beta} = \mathbf{v}/c$ is the dimensionless particle velocity. The radiation friction force is inversely proportional to the particle mass. We can therefore assume that only electrons are responsible for the radiation because of their low mass compared to ions. In that case the radiated power reads $P_{re} = \tau_r m_e w_e^2$, where $\tau_r = 2\,e^2/3m_e c^3 \simeq 6.2\times10^{-24}$ s is the characteristic time and $\mathbf{w_e}$ is the electron acceleration. In the relativistic case, it is concentrated around a cone with an angle $\sim 1/\gamma$. The radiation spectrum is discussed in Sec. II B.

This radiation takes away from the electron and from the laser field momentum and energy. These effects need to be accounted for in the electron equation of motion. In the covariant relativistic approach developed by Dirac, it is represented by the self-force four-vector F^μ_{sf} that is added to the Lorentz four-force F^μ_{Le}. Then the electron equation of motion takes the form:

$$m_e c\,\dot{u}^\mu = F^\mu_{Le} + F^\mu_{sf}, \tag{2}$$

where $u^\mu = (\gamma_e, \gamma_e\beta_e)$ is the electron four-velocity, $F^\mu_{Le} = -(e/c)\,\mathcal{F}^{\mu\nu}u_\nu$ is the Lorentz force (1) related to the electromagnetic stress tensor $\mathcal{F}_{\mu\nu} = \partial A_\mu/\partial x^\nu - \partial A_\nu/\partial x^\mu$, $-e$ is the electron charge, and $F^\mu_{sf} = m_e\tau_r(\ddot{u}^\mu - u^\mu u^\nu \ddot{u}_\nu)$ is the self-force.

It was thus suggested in [11] to neglect it in the zeroth order, express then the acceleration with the Lorentz force, and inject this expression in the self-force tensor. It then takes the following form:

$$F^\mu_{sf} = -e\tau_r\frac{\partial\mathcal{F}^{\mu\nu}}{\partial x^\sigma}u_\nu u^\sigma - \frac{e^2\tau_r}{m_e^2c^2}\mathcal{F}^{\mu\nu}\mathcal{F}_{\nu\sigma}u^\sigma + \frac{e^2\tau_r}{m_e^2c^2}\mathcal{F}_{\nu\sigma}u^\sigma\mathcal{F}^{\nu\varrho}u_\varrho u^\mu. \tag{3}$$

This term is supposed to be small compared to the Lorentz force in the electron proper reference frame. The radiation reaction may have a significant effect on the electron dynamics only in the relativistic limit, $\gamma_e \gg 1$. In that case, the third term in the right-hand side of Eq. (3) is of the order of $\gamma_e^2 \gg 1$. It is therefore the dominant term. Moreover, the first term containing the field derivatives is smaller than the two other terms and may be comparable to the electron spin corrections. This fact has been discussed in Ref. [13]. Returning to the three-vector formulation and neglecting the first term in Eq. (3), such a simplified version of the equations of electron motion writes

$$\frac{d\mathbf{p}_e}{dt} = \mathbf{F}_{Le} + \mathbf{F}_{sf}, \quad \frac{d\mathbf{x}_e}{c\,dt} = \boldsymbol{\beta}_e,$$
$$\text{where}\quad \mathbf{F}_{sf} = -\frac{e\tau_r}{m_e c}[\mathbf{F}_{Le}\times\mathbf{B} - e\mathbf{E}\,(\boldsymbol{\beta}_e\cdot\mathbf{E})] - \frac{\tau_r}{c}\,\gamma_e^3\boldsymbol{\beta}_e(\mathbf{w}_e\cdot\mathbf{F}_{Le}). \tag{4}$$

Compared to the LAD model, this system of equations does not contain the self-accelerating solutions and can be conveniently applied for numerical simulations of multiparticle systems [13].

Recently, the authors of Refs. [17,18] proposed an improved model for the radiation reaction force that has better properties of energy and momentum conservation and can be extended to higher values of the parameter $\chi_e < 1$. The corresponding equations of electron motion read

$$\frac{d\mathbf{p}_e}{dt} = \mathbf{F}_{Le} - e\,\delta\boldsymbol{\beta}_e\times\mathbf{B} - \gamma_e^2(\mathbf{F}_{Le}\cdot\delta\boldsymbol{\beta}_e)\boldsymbol{\beta}_e, \tag{5}$$

$$\frac{d\mathbf{x}_e}{c\,dt} = \boldsymbol{\beta}_e + \delta\boldsymbol{\beta}_e, \tag{6}$$

where the radiation losses are described by the correction term to the electron velocity

$$\delta\boldsymbol{\beta}_e = \frac{(\tau_r/c)\,\gamma_e\mathbf{w}_e}{1 - (e\,\tau_r/m_e c)\,(\boldsymbol{\beta}_e\cdot\mathbf{E})}. \tag{7}$$

Here, the second term in the denominator accounts for the saturation of the radiation losses in intense fields. However, as discussed in Ref. [19], its contribution is negligible even at the upper limit of classical electrodynamics. Its relative

value, $\omega_L \tau_r a_L$, is of the order of 10^{-5}. The second term in the right-hand side of Eq. (5) induces a deviation of the electron momentum and can be thought as a modification of the curvature of the electron orbit. The last term in the right-hand side of this equation can be identified as a friction force as it is directed in the direction opposite to the particle velocity. In the first order on the radiation parameter τ_r this term reduces to the second term in the self-force of the LL model (4). The numerical implementation of the radiation force model is described in the next section.

B. Spectrum of radiation emission

The radiation force is related to the incoherent emission of high-frequency radiation by electrons. The radiation spectrum consists of the harmonics of the laser frequency shifted by the Doppler effect. There could also be harmonics of the Doppler-shifted electron cyclotron frequency if a magnetic field is present. We assume that each electron radiates independently and contributions of all electrons are added incoherently. This assumption works if the distance between each electron ($d_e \simeq n_e^{-1/3}$) is larger than the characteristic radiation wavelength, for each electron ($\lambda_{cr} \simeq \frac{2\pi c}{\omega_{cr}}$), which is the case in our simulations. Moreover this assumption is used in the part describing the kinetic equations. It ensures the nondivergence in the source term of the kinetic equation of photons (see part C of Sec. II).

The exact expression of the radiation spectrum can be significantly simplified in the ultrarelativistic limit. The instantaneous electron motion can be represented as a sum of the rectilinear motion characterized by the relativistic factor γ_e and a circular motion characterized by the rotation frequency $\omega_r = |\mathbf{p}_e \times \mathbf{F}_{Le}|/p_e^2$. In the limit $\gamma_e \gg 1$ the radiation spectrum can be approximated by a continuous function $S(\omega/\omega_{cr})$, where $\omega_{cr} = \frac{3}{2}\omega_r \gamma_e^3$ is the critical frequency defining the maximum of the spectrum, $S(r) = 3^{5/2}(8\pi)^{-1} r \int_r^\infty K_{5/3}(r')\, dr'$ defines the spectral shape, and $K_{5/3}$ is a modified second-order Bessel function. The function $S(r)$ is normalized as $\int_0^\infty S(r)\, dr = 1$.

The radiation is emitted in a cone with the angle $\sim 1/\gamma_e$ with respect to the electron propagation direction. Because in the ultrarelativistic limit this angle is rather small and the number of emitting electrons is large, it is sufficient for numerical modeling to assume that photons are emitted in the direction of electron propagation. Then the intensity of emitted radiation by a single electron can be presented as follows [7,19]:

$$\frac{d^2 I_r}{d\omega d\boldsymbol{\Omega}} = \frac{\gamma_e^3 \tau_r}{\omega_{cr}} (\mathbf{F}_{Le} \cdot \mathbf{w}_e)\, \delta\left(\boldsymbol{\Omega} - \frac{\mathbf{p}_e}{p_e}\right) S\left(\frac{\omega}{\omega_{cr}}\right). \quad (8)$$

By integrating this formula over the spectrum and the emission directions represented by the unitary vector $\boldsymbol{\Omega}$, one finds the total radiated power determined by the Larmor formula. It is supposed in the present model that the radiation escapes freely from the plasma, not interacting with the plasma particles. Numerically, the radiation of all electrons is collected at each time step and then integrated over the observation time.

C. Kinetic equations for the particles

The single-particle dynamics described above can be incorporated in the kinetic model describing a collective motion of the plasma in the radiation field. The plasma dynamics is described by a set of kinetic equations for the distribution functions of electrons, $f_e(\mathbf{p}_e)$, ions $f_i(\mathbf{p}_i)$, and photons $f_\gamma(\mathbf{p}_\gamma)$ [22]. In the domain of classical electrodynamics, $\chi_e < 1$, these equations read

$$\begin{aligned}
&\frac{\partial f_e}{\partial t} + c\boldsymbol{\beta}_e \cdot \nabla f_e + \mathbf{F}_{Le} \cdot \frac{\partial f_e}{\partial \mathbf{p}_e} = \frac{\tau_r}{c} \frac{\partial}{\partial \mathbf{p}_e} \cdot \left[\gamma_e^3 \boldsymbol{\beta}_e (\mathbf{w}_e \cdot \mathbf{F}_{Le}) f_e\right], \\
&\frac{\partial f_i}{\partial t} + c\,\boldsymbol{\beta}_i \cdot \nabla f_i + \mathbf{F}_{Li} \cdot \frac{\partial f_i}{\partial \mathbf{p}_i} = 0, \\
&\frac{\partial f_\gamma}{\partial t} + c\,\boldsymbol{\Omega} \cdot \nabla f_\gamma \\
&\quad = \frac{\tau_r c^3}{\hbar^4 \omega^3} \int d\mathbf{p}_e\, f_e(\mathbf{p}_e) \frac{\gamma_e^3}{\omega_{cr}} (\mathbf{w}_e \cdot \mathbf{F}_{Le}) \delta\left(\boldsymbol{\Omega} - \frac{\mathbf{p}_e}{p_e}\right) S\left(\frac{\omega}{\omega_{cr}}\right).
\end{aligned} \quad (9)$$

Here, the photon momentum is defined as $\mathbf{p}_\gamma = \boldsymbol{\Omega}\hbar\omega/c$ and the photon energy density is $\mathcal{E}_\gamma = \int d\mathbf{p}_\gamma\, \hbar\omega\, f_\gamma$. The terms in the left-hand side of these equations are describing the transport of particles in the phase space. The radiation terms are presented as sources in the right-hand side of the kinetic equations for electrons and photons. As we did not find any significant difference between the models (4) and (5) in the domain of applicability of the classical electrodynamics (see also the next section), the simplified LL model containing only the friction term in the self-force is incorporated in the electron kinetic equation. The radiation reaction term conserves the number of electrons, and it accounts for the energy and momentum losses. It has the form of a friction force in a standard Fokker-Planck equation, but the divergence of the friction force in the momentum space is nonzero, $\partial \mathbf{F}_{sf}/\partial \mathbf{p}_e < 0$. This leads to the contraction of the electron distribution function in the phase space as discussed in Ref. [23]. The self-force is related to a spontaneous radiation; thus it does not depend on the number of photons. In the photon kinetic equation, the right-hand side describes the local contribution of all electrons in the photon generation in the direction $\boldsymbol{\Omega}$ with the energy $\hbar\omega$ according to Eq. (8).

The system of equations (9) describes the exchange of momentum and energy between electrons and photons. This radiation emission process is complementary to the electron motion in the electromagnetic field described by the Lorentz force in the left-hand side of the electron kinetic equation. Such a scheme opens the possibility of accounting for short-wavelength radiation that cannot be described classically by Maxwell's equations. Indeed, the computational grid in PIC codes limits the spectrum of electromagnetic radiation to $\omega < c/\Delta$, where Δ is the grid size. In practical terms the code usually does not resolve photon energies larger than $\sim$100 times the laser photon energy. The corpuscular model described by the third equation of system (9) accounts for photons with larger energies and its contribution in the domain described by Maxwell's equations should be negligible. According to the spectrum (8), the corresponding condition reads $\omega_{cr} \gg c n_e^{-1/3}$. It limits the applicability of our model to relativistic electrons only and to energetic part of the electromagnetic spectrum of a few kilo-electron-volts or more. Moreover, the system of kinetic equations (9) is valid within the limits of the classical electrodynamics $\chi_e \ll 1$ and for plasmas of a relatively small size transparent to the radiation. It can be extended further to account for secondary effects

such as Compton scattering, pair production, and stimulated photon emission and absorption.

III. NUMERICAL APPROACH

A. Implementation of the self-force

The radiation effects are implemented in the one-dimensional (1D) version of the code PICLS [21] according to Eqs. (5). An important particularity of the PICLS code is that modeling of plasma density gradients is done with particles of variable weights. In the present version binary collisions between particles are neglected. Moreover, we use fourth-order interpolation for the numerical solver proposed in the paper to apply fields and deposit currents.

The radiation losses are implemented at the first substep of the time loop while solving the equations of motion for electrons. For that the original numerical scheme of PICLS was modified as follows. The electron momentum at time step $n+1$ is updated by adding the radiation reaction term calculated explicitly knowing the corresponding values at the previous time step:

$$\begin{aligned} \boldsymbol{p}_e^{n+1} &= \tilde{\boldsymbol{p}}_e^{\,n+1} - \delta \boldsymbol{p}_e^n, \\ \delta \boldsymbol{p}_e^n &= \frac{1}{m_e c} \tilde{\gamma}_e^{\,n+1} \left(\delta \tilde{\boldsymbol{\beta}}_e^{n+1} \cdot \boldsymbol{F}_{Le}^{n+1} \right) \tilde{\boldsymbol{p}}_e^{\,n+1} \Delta t \\ &\quad + \delta \tilde{\boldsymbol{\beta}}_e^{\,n+1} \times \boldsymbol{B}^{n+1} \Delta t, \end{aligned}$$

where $\tilde{\mathbf{p}}_e^{n+1}$ is the electron momentum calculated implicitly while taking into account only the Lorentz force. $\delta \boldsymbol{p}_e^n$ is the electron momentum correction due to radiation losses and is calculated after the application of the Lorentz force. This term implies a reduction of the volume of the electron phase space. This point has been discussed in the kinetic equation part. A similar procedure was applied for the calculation of the coordinates:

$$\begin{aligned} \mathbf{x}_e^{n+1} &= \tilde{\mathbf{x}}_e^{n+1} + \frac{\mathbf{p}_e^{n+1}}{\gamma^n m_e} \Delta t, \\ \mathbf{x}_e^{n+1} &= \tilde{\mathbf{x}}_e^{n+1} - \frac{\gamma_e^n}{m_e} \boldsymbol{\beta}_e^n \left(\delta \boldsymbol{\beta}_e^n \cdot \mathbf{F}_{Le}^n \right) (\Delta t)^2. \end{aligned}$$

It is clear that the contribution of the third term defining electron momentum is negligible in the calculation of the coordinates. Our approach for the numerical implementation of radiation losses is similar to the one described in [13]. The main difference is that momentum variations due to radiation losses is calculated explicitly knowing the particle momentum at the previous time step. The numerical scheme used to move the particles is similar to the Boris pusher [24]. This method for the calculation of the particle momentum allows us to minimize numerical errors in the dynamics of charged particle determined by electromagnetic fields. The radiation force is calculated with the same pusher that calculates the Lorentz force. This additional calculation does not affect the stability of the numerical scheme, if the condition $\omega_{pe} \Delta t < 2$ is fulfilled, where ω_{pe} is the characteristic plasma frequency. For numerical simulations in underdense plasmas and at high laser intensities fast electron radiation cooling may also limit the time step.

B. Importance of radiation losses at ultrahigh laser intensities

In order to show the performance of this numerical scheme, we compared the difference in computation time for one-dimensional runs with and without radiation losses. We considered a laser pulse with a circular polarization, an amplitude $a_L = 192$, and a wavelength $\lambda_L = 0.8\,\mu$m normally incident on a plasma layer with the electron density $n_e = 100\, n_c$, where $n_c = m_e \omega_L^2 / 4\pi e^2$ is the critical density. Both thick, $l = 100\,\lambda_L$, and thin, $l = \lambda_L/8$, plasmas were considered. For the case of a thin target the relative difference in computing ~20 000 time steps is 2.8%, while for a thick target it increases to 8.4% including input and output. Therefore, implementation of radiation losses in the code does not penalize its performances. More complicated runs require more computations, but the relative difference remains in the range of 20–30%, which is an acceptable value.

In order to demonstrate the role of radiation losses in laser plasma interaction, we calculated the radiated energy for similar interaction conditions while changing the laser amplitude from $a_L = 10$ to 450. The plasma layer with the electron density $n_e = 10\, n_c$ and a thickness of $l = 100\,\lambda_L$ was surrounded by 10-λ_L-long vacuum regions from both sides of the simulations box. The laser pulse has a trapezoidal profile with a linear ramp of one laser period $T_L = \lambda_L / c$ and a constant section of 16 T_L. Each plasma cell has the size of $1/100\,\lambda_L$ and it contains 30 macroparticles, electrons and ions, with the mass ratio $m_i/m_e = 3600$.

In Fig. 1, for relatively low laser intensities below 10^{22} W/cm^2 the radiated energy 0.1 J/cm^2 is negligible compared to the incident laser energy of 5×10^8 J/cm^2, and the radiation force has no influence on the plasma dynamics. However, the difference becomes significant for higher laser intensities. In the extreme case of 3.3×10^{23} W/cm^2 the radiated power is comparable to the incident laser power. Moreover, the radiation losses continue even after the end of the laser pulse due to the remaining electrostatic field, although the radiation power strongly decreases.

We also evaluated the difference between models (4) and (5) by performing the same simulations as above with model (5). Figure 2 shows the ion phase space obtained at the time $t = 50\, T_L$ in these runs. For the two considered laser intensities of 8×10^{22} W/cm^2 and 3.3×10^{23} W/cm^2 there are practically no differences in the ion distribution and in the electron trajectories. We conclude that for laser intensities within the classical limit $\chi_e < 1$ it is not necessary to take into account the modification of the electron trajectory in the second equation of system (5) and both models give essentially the same results.

C. Test cases

Our implementation of the radiation effects was also verified by a comparison of our simulations with two cases published in Refs. [7,14]. Here, only comparisons with [7] are presented. In this first case, hole boring in a thick plasma layer by a laser pulse is considered. The following set of parameters was taken from Ref. [7]. The laser parameters are $\lambda_L = 0.8\,\mu$m, $I_L = 4 \times 10^{22}$ W/cm^2, linear polarization, and a constant intensity with 2 T_L rising edge. The plasma parameters are the following: ion-to-electron mass ratio $m_i/m_e = 3600$,

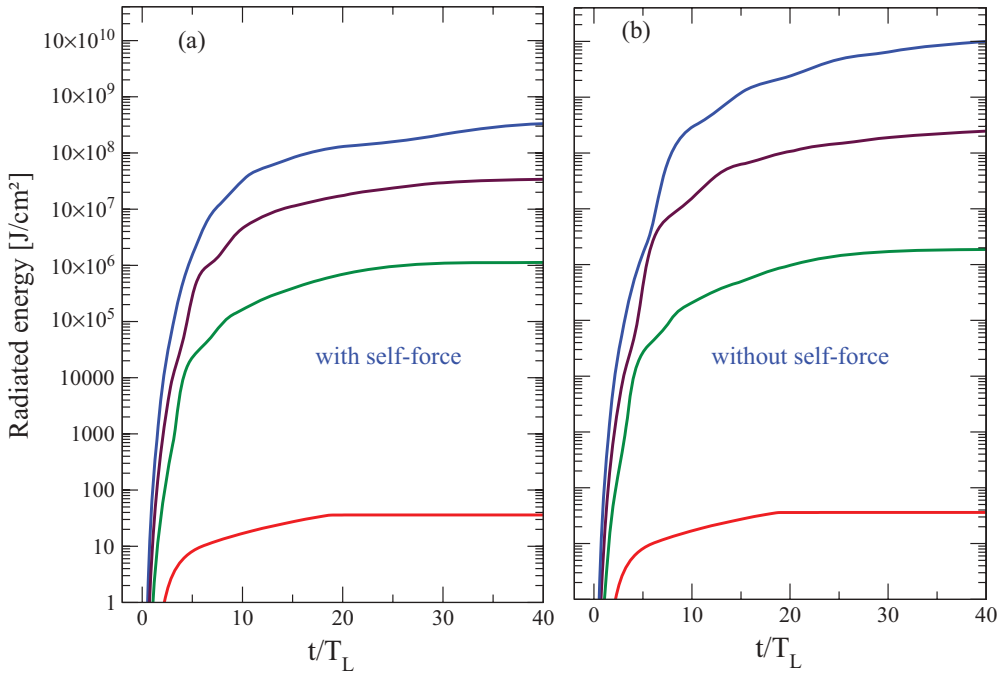

FIG. 1. (Color online) Radiation losses from a laser plasma interaction with (a) and without (b) accounting for the self-force for the laser intensities (from bottom to top) 10^{21} W/cm^2 (red), 10^{22} W/cm^2 (green), 8×10^{22} W/cm^2 (violet), and 3.3×10^{23} W/cm^2 (blue). Other parameters are given in the text.

ion charge $Z = 1$, electron density $n_e = 10\, n_c$, and initial electron temperature $T_e/m_e c^2 = 10^{-2}$. The target with a thickness $l = 100\, \lambda_L$ was surrounded by 10-λ_L-long vacuum regions on both sides of the simulations box. $t = 0$ is chosen as the time when the laser pulse penetrates the plasma layer.

Figure 3 shows the phase space of electrons with and without radiation losses at $t = 100\, T_L$. General features of the electron and ion phase space are very similar to the results presented in Ref. [7]. The radiation losses lead to electron cooling and to a decrease of the phase space volume. The maximum electron momentum is reduced from $1500\, m_e c$ to less than $800\, m_e c$, and the maximum ion backward momentum is decreased from $-0.9\, m_i c$ to $-0.1\, m_i c$.

Additional information can be obtained from this test case. The radiation effects can also be seen in the charge separation electric field presented in Fig. 4. Indeed, in the case with radiation losses the number of escaping electrons in the zone $x < 0$ is much smaller and the electrostatic field E_x is almost zero. This explains the massive reduction in backward electron acceleration when radiation losses are taken into account.

By preventing strong electron heating, the radiation losses reduce the electron thermal pressure and consequently the

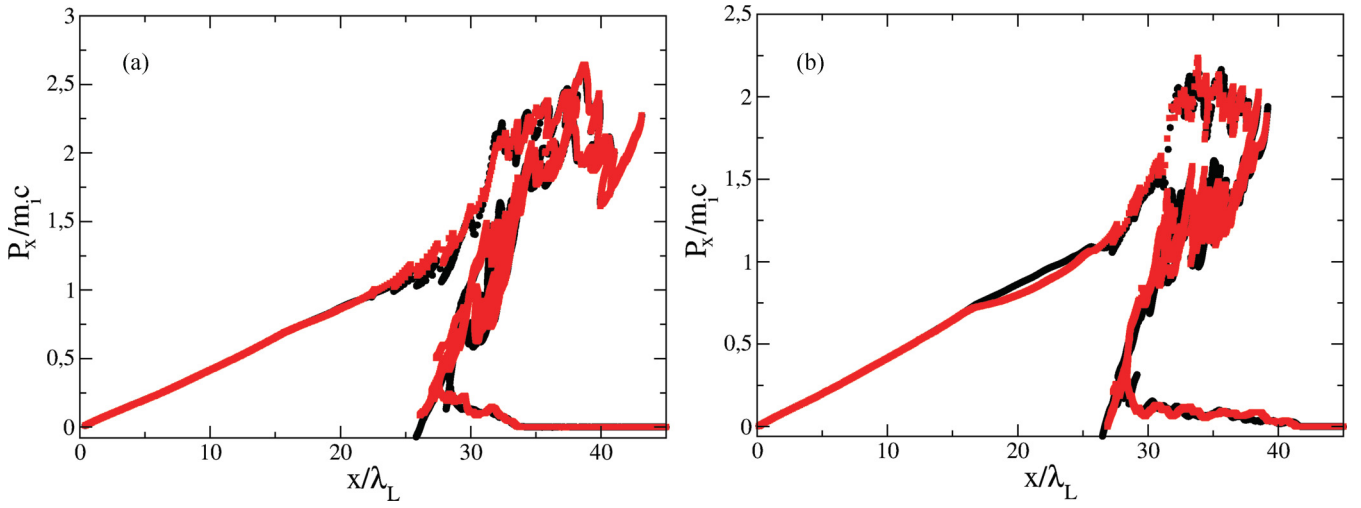

FIG. 2. (Color online) Ion phase space showing the difference between the models accounting for the radiation effects for the laser intensity 8×10^{22} W/cm^2 (a) and 3.3×10^{23} W/cm^2 (b). Red (gray) squares denote simulation with the radiation force model described by Eqs. (5). Black circles denote simulation with the radiation force model described by Eqs. (4). The laser and plasma parameters are the same as in Fig. 1.

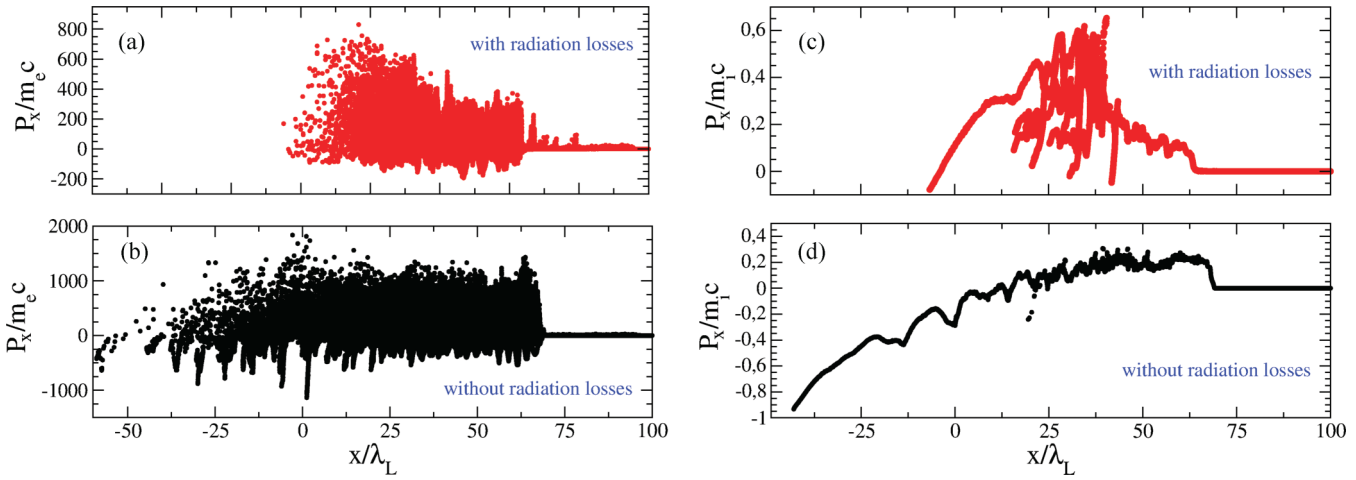

FIG. 3. (Color online) Distribution of electrons (a, b) and ions (c, d) in the phase space with (a, c) and without (b, d) radiation losses at $t = 100\,T_L$. The parameters of simulation taken from Ref. [7] are given in the text.

thickness of the electron layer. This makes ion acceleration more effective in this setup using a long overdense target with a density close to the critical density. Indeed, as can be seen in Fig. 3(d), the ion momentum in the backward direction is reduced and it is increased in the forward direction. Ion acceleration through the radiation pressure is even stronger for the circularly polarized laser where the oscillating component of the Lorentz force vanishes and generation of fast electrons is suppressed. Typically, with radiation losses in the linear polarization case, we find the maximum ion momentum max $p_i \simeq 0.7\,m_i c$, whereas max $p_i \simeq 1.5\,m_i c$ in the circular polarization case.

The manifestations of radiation losses depend strongly on the laser polarization. In the circular polarization case, the radiation losses are relatively small. They slightly increase the laser absorption coefficient and thus decrease the piston velocity. This is demonstrated in more detail in the next section. In the linear polarization case, the oscillating component in the Lorentz force increases the parallel momentum of electrons in the piston. Some electrons can escape the laser piston, emit radiation, and cool down. The electrons remaining in the piston are better compressed and improve ion acceleration due to a stronger longitudinal field.

Knowing the electron acceleration $\mathbf{w_e}$ (7) one may evaluate the rate of radiation losses along the trajectory. For electrons propagating opposite to the laser, radiation losses are maximal. They can be estimated as $\sim\omega_L^2\tau_e\gamma_e^2 a_L^2 m_e c^2$. The rate of radiation losses of electrons moving in the perpendicular direction is smaller by a factor of γ_e^2. This dominance of the radiation losses for backward-propagating electrons is demonstrated in Fig. 5, where the radiation efficiency is maximal for electrons with a small perpendicular momentum.

Our results are also in good agreement with the simulation results published in [14], even if the implementation of radiation losses is not exactly the same. Moreover, we confirm

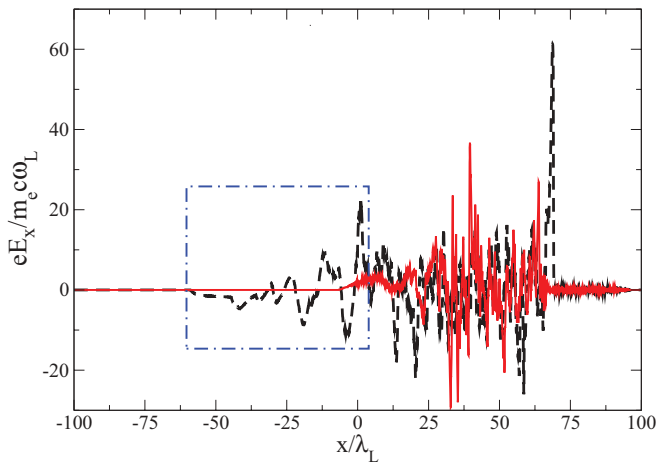

FIG. 4. (Color online) Charge separation field with (red [gray] lines) and without (black dashed lines) radiation losses at $t = 100\,T_L$. The simulation parameters are given in the text. The part of the electric field outside the plasma is shown in the dash-dotted frame.

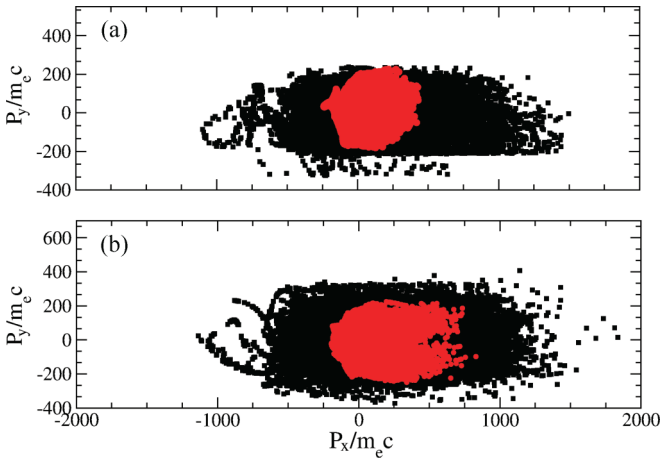

FIG. 5. (Color online) Influence of radiation losses on the electron distribution function in the perpendicular, p_y, and parallel, p_x, momenta phase space in a thick target with a density of $10\,n_c$ at $t = 100\,T_L$ for a circular (a) and linear (b) polarization of the laser light with $a_L = 192$. Red (gray) circles and black squares represent the electron distribution in the run with and without radiation losses, respectively.

that our code conserves total energy when taking into account radiation losses. Numerical solutions for a counterpropagating electron in a plane wave and also in a uniform and constant magnetic field are in a good agreement with the analytical solutions [17].

IV. ION ACCELERATION AT ULTRAHIGH LASER INTENSITIES

Starting from the interaction parameters presented in the previous section, we investigated the effect of radiation losses in more detail on laser ion acceleration under the conditions where radiation pressure acceleration (RPA) is a dominant process. The following laser parameters were considered: $\lambda_L = 0.8\,\mu$m, $I_L = 8 \times 10^{22}$ W/cm^2, circular polarization, and a trapezoidal temporal profile with a linear front during one laser period and a constant section of $16\,T_L$. The ion-to-electron mass ratio is $m_i/m_e = 3600$, the ion charge is $Z = 1$, and the initial electron temperature is $T_e/m_e c^2 = 10^{-2}$. Plasma layers of three thicknesses were considered, $l = 1/8\,\lambda_L, 0.5\,\lambda_L$, and $100\,\lambda_L$. Plasma density varied between 10 and 100 n_c.

Figure 6 shows how the efficiency of radiation losses depends on the interaction regime. For a thin target, the effect of radiation losses on ion acceleration is relatively weak. There is practically no difference for a dense target with $n_e = 100\,n_c$ and $l = 0.5\,\lambda_L$ [panel (c)], while ions lose more energy in the case of a thinner target, $l = 1/8\,\lambda_L$ [panel (a)]. This latter regime corresponds to the case of relativistic transparency, where the target areal density ξ

$$\xi = \pi \frac{n_e}{n_c} \frac{l}{\lambda_L} \tag{10}$$

is smaller than the laser amplitude. This parameter has been discussed in Refs. [25,26] in the context of radiation pressure acceleration and Coulomb explosion. The lower ion energy observed in the case of a dense and thin target shown in Fig. 6(a) can be explained by the fact that when radiation losses are included, electron heating is weaker and the electrons are better compressed by the laser ponderomotive force, forming a thin and dense charge sheet. The charge separation electric field shown in Fig. 7 has a more regular structure and its maximal amplitude increases by around 40% when radiation losses are taken into account for the case $a_L = 136$. This regime of acceleration can be associated with a directed Coulomb explosion, because almost all electrons in such a thin target are pushed forward and separated from ions. The accelerating electric field is spread over the whole target, leading to a broad ion energy spectrum.

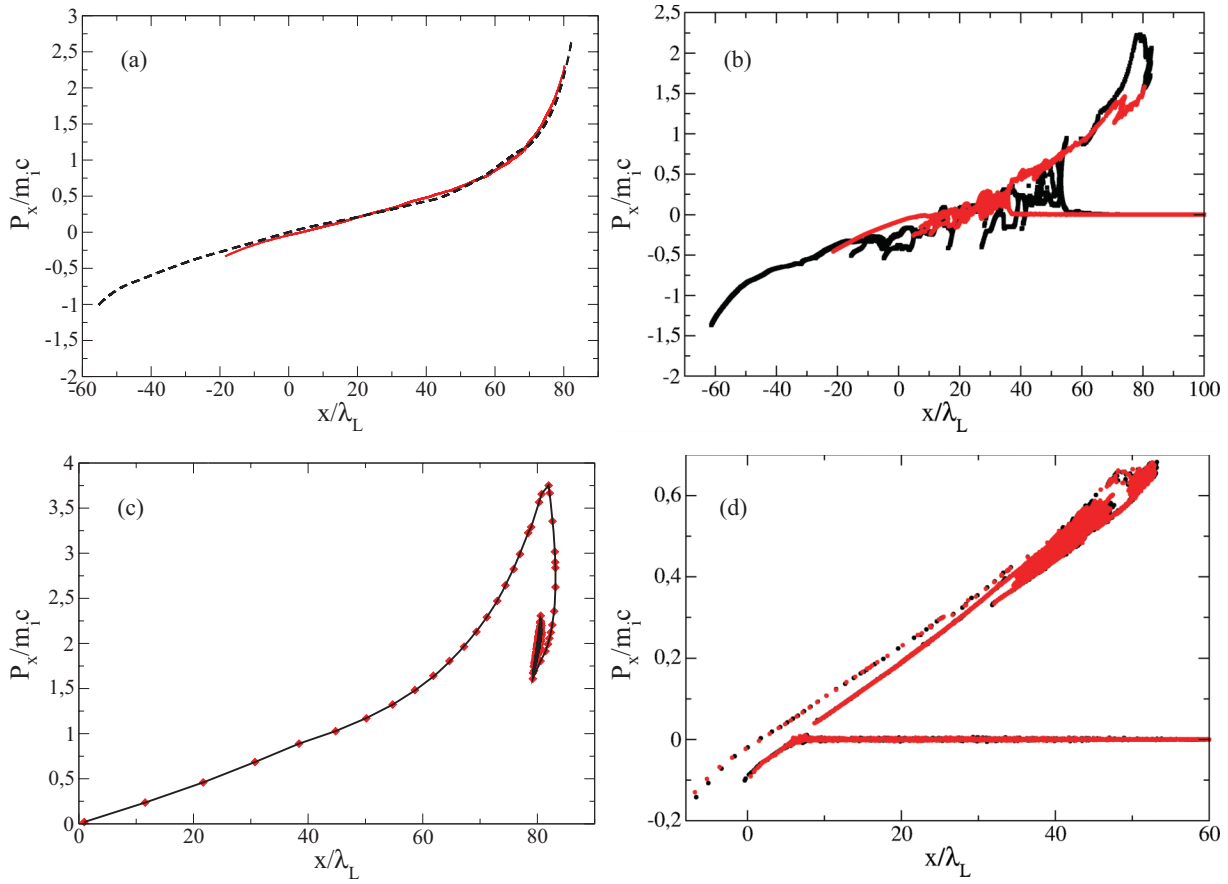

FIG. 6. (Color online) Effects of radiation reaction on the ion phase space at time $t = 100\,T_L$: for a target density of $100\,n_c$ with the thickness $1/8\,\lambda_L$ (a) and $0.5\,\lambda_L$ (c); and for a target thickness of $100\,\lambda_L$ with the density $10\,n_c$ (b) and $50\,n_c$ (d). Different regimes of ion acceleration are presented: a directed Coulomb explosion (a), the induced transparency regime (b), the light sail regime (c), and the piston regime (d). Red (gray) lines and red (gray) circles (black dashed lines and black squares) represent the cases with (without) radiation losses.

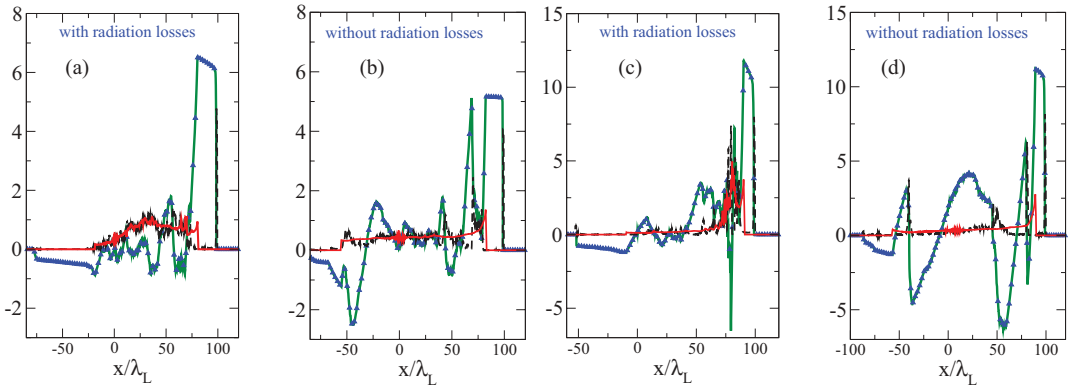

FIG. 7. (Color online) Distribution of the electron (black dashed lines) and ion (red [gray] lines) densities and the electrostatic field (green lines with blue triangles up) in the case of a thin target $l = 1/8\,\lambda_L$ and $n_e = 100\,n_c$ at time $t = 100\,T_L$ for the laser amplitude $a_L = 136$ (a, b) and $a_L = 263$ (c, d). The cases with (a, c) and without (b, d) radiation losses are shown. The densities are normalized by the initial density divided by 500; the electric field is normalized by the factor $m_e\omega_L c/e$.

The corresponding electron energy distribution is shown in Fig. 8(c). Electrons with energies of several hundred million electron volts are those which have escaped the target and interacted strongly with the laser field. These electrons are radiating their energy very efficiently. For this reason the maximum electron energy is limited to 125 MeV

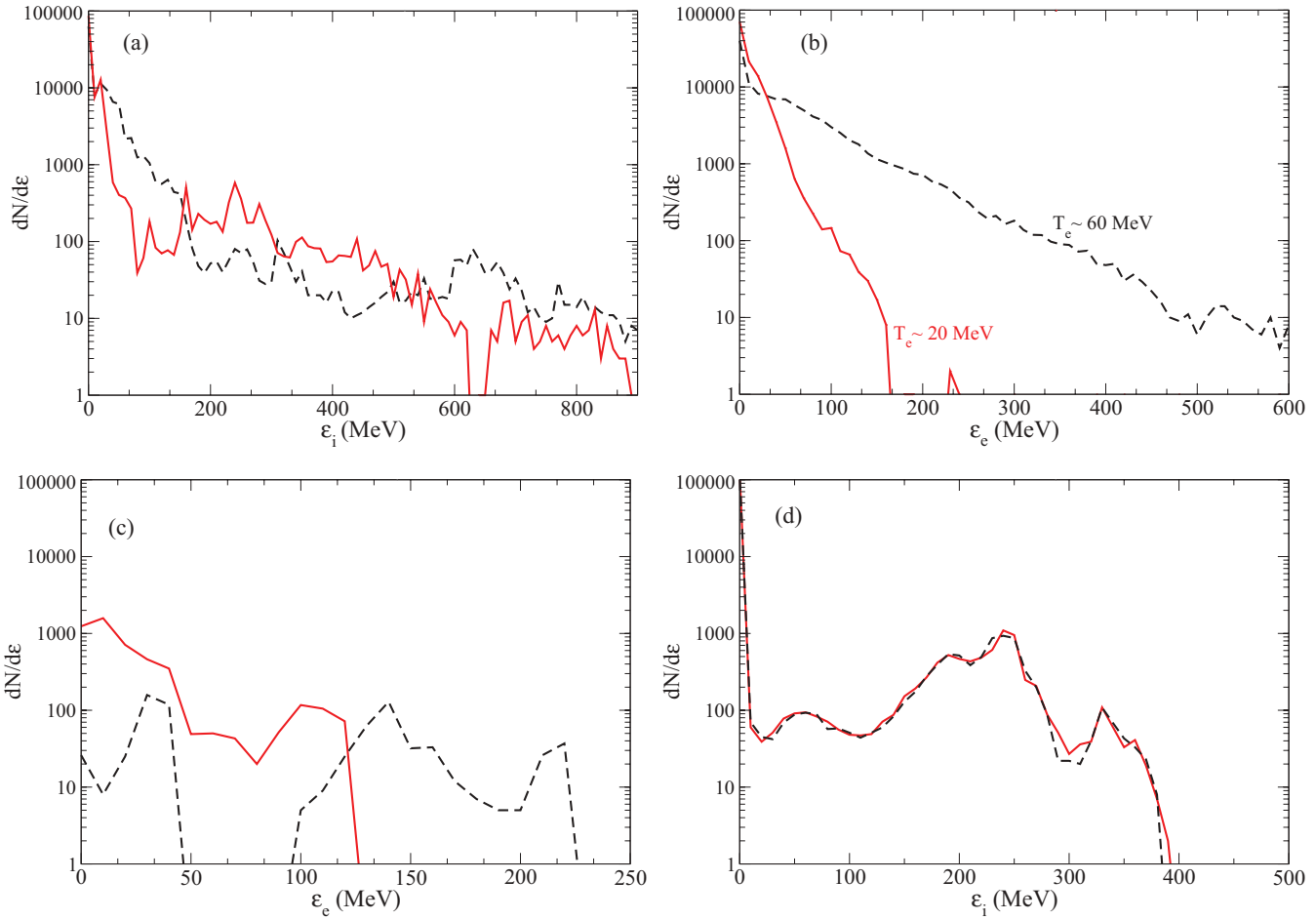

FIG. 8. (Color online) Effect of radiation losses on the ion and electron energy distribution at time $t = 100\,T_L$: ion (a) and electron (b) energy distribution for the target with $l = 100\,\lambda_L$ and $n_e = 10\,n_c$; (c) electron energy distribution for the target with $l = 1/8\,\lambda_L$ and $n_e = 100\,n_c$; (d) ion energy distribution for the target with $l = 100\,\lambda_L$ and $n_e = 50\,n_c$. Red (black dashed) lines represent the cases with (without) radiation losses.

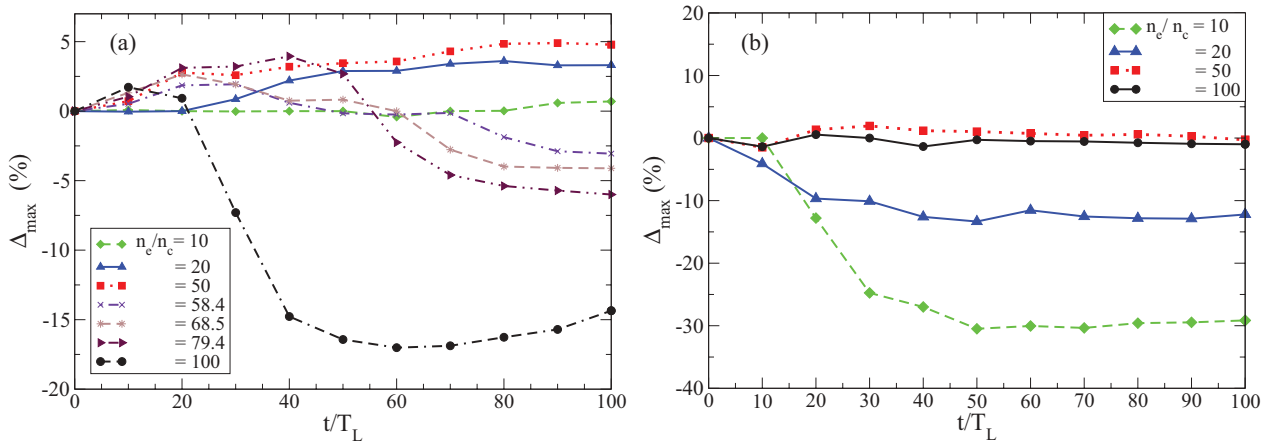

FIG. 9. (Color online) Time dependence of the effect of radiation losses for thin $l = 0.125\,\lambda_L$ (a) and thick $l = 100\,\lambda_L$ (b) targets of different densities. The laser amplitude is $a_L = 136$. The plasma densities are given in the legend.

in the simulation with radiation losses. Without radiation losses, two peaks in the electron energy distribution shown in Fig. 8(c) very likely correspond to two spatially distinct groups. The low-energy electrons are sitting at the front of the laser pulse and moving with ions, while the more energetic ones are those lagging behind and oscillating in a strong laser field. In the case with radiation losses, these two groups of electrons are less separated. The most energetic electrons are cooling down due to radiation losses, so the energy and the number of hot electrons decrease. Consequently, the number of low-energy electrons increases, as can be seen in Fig. 8.

The laser pulse reflectivity from a thin foil depends on the ratio between its dimensionless areal density called ξ (10) and the dimensionless laser amplitude a_L [27,28]. In the high-density case, Fig. 6(a), the parameter $\xi \simeq 39$ is much smaller than the laser amplitude $a_L \simeq 136$. The foil is therefore effectively transparent for the laser radiation. The electrons are pushed forward by the laser light and ions are trailing behind. The case of an even higher laser amplitude $a_L = 263$ shown in Fig. 7(b) is more beneficial for efficient acceleration of ions. The radiation losses allow for the electrons to stay in front of the laser pulse. Otherwise they would be heated up, demonstrating a chaotic motion, and left behind the laser pulse, creating a wake.

The areal density of a high-density target, $\xi \simeq 160$, shown in Fig. 6(c) is larger than the laser amplitude $a_L \simeq 136$. Correspondingly, the electrons and ions are moving together as a light sail [23,29]. The radiation losses are relatively small in that case as the laser field and particles are spatially well separated.

The regime of a thick target at a relatively low density, $l = 100\,\lambda_L$ and $n_e = 10\,n_c$, is marginal between hole boring and relativistic transparency. As the relative electron density n_e/n_c is smaller than the laser dimensionless amplitude, $a_L \simeq 136$, the laser light penetrates partially in the plasma. Nevertheless, the piston is formed behind the front of the laser pulse. The ion energy distribution in this case, shown in Fig. 8(a), is not too sensitive to electron radiation losses. The ions escaping from the target towards the laser see a smaller electrostatic field because of electron cooling and consequently attain much smaller energies [Fig. 6(b)]. This electron cooling is clearly visible in the electron energy distribution, as it is shown in Fig. 8(b). The electron distribution is close to a Maxwellian function, and the radiation cooling reduces the hot electron temperature from 60 to 20 MeV, more than three times.

Ion acceleration in a thick and dense target, $n_e = 50\,n_c$ [Fig. 6(d)], proceeds in the so-called hole-boring regime. The ions are accelerated to the velocity $v_{i\,\max} = 2\,v_b$ in the piston, where $v_b \approx \frac{1}{2} a_L c \sqrt{m_e n_c / m_i n_i}$ is the piston velocity. In this case the electron density profile is very steep; very few electrons are escaping the piston. The electromagnetic fields and the particles are spatially separated, and the radiation losses are very low. The ion energy distribution in the high-density case, Fig. 8(d) agrees well with the standard picture of the laser piston. There are two ion groups: one consists of cold ions upstream of the piston that are not yet accelerated. Another group consist of fast ions with velocities approximately twice the piston velocity.

The effect of electron radiation losses on ion acceleration can be characterized by the dimensionless parameter $\Delta_{\max}$, which is the relative gain of the maximum ion momentum:

$$\Delta_{\max} \equiv \frac{\max p_{i,\mathrm{rad}} - \max p_{i,\mathrm{no\,rad}}}{\max p_{i,\mathrm{no\,rad}}}. \qquad (11)$$

The dependence of this parameter with time is presented in Fig. 9. For the case of a thin target [same parameters as described in Fig. 6(a)], the laser pulse crosses the target and strips out a relatively small part of electrons from its rear side. This can be clearly seen in Fig. 7. The radiation losses of these accelerated electrons enable their better confinement in the front of the laser pulse and improve ion acceleration from the rear side of the target. For these reasons the parameter $\Delta_{\max}$ is positive initially, but its sign changes with time.

This is due to two effects. First, the number of electrons trapped in the front of the laser pulse decreases with time as they return to the target. The radiation losses are due to the electrons propagating versus the laser. So, they are losing their momentum and decrease the charge separation electric field. Second, the electrons that remain in the target are heated by the laser and their radiation losses increase with time. Correspondingly, the intensity of the transmitted laser pulse decreases with time as well as the efficiency of ion acceleration.

Obviously, as the target density is higher, the radiation losses become stronger and ion acceleration is less efficient. Thus $\Delta_{\max}$ is negative and its absolute value increases with the target density. This explanation is confirmed by the electron energy spectrum shown in Fig. 8(c). In the case with radiation losses, electrons are less energetic and the number of hot electrons is smaller.

For the case of a thick target, $l = 100\,\lambda_L$ [Fig. 9(b)], the parameter $\Delta_{\max}$ is essentially negative and it attains a quasistationary value after a few tens of laser periods. The radiation effect attains the value of $\sim$30% in the regime of a partial target transparency, where the laser penetrates sufficiently deep in the target. This effect decreases with the target density. For densities exceeding $50\,n_c$, the interaction takes place in the piston regime, where the laser radiation is well separated from electrons. The radiation losses are thus small and they decrease with the plasma density, having almost no effect on ion acceleration.

This explanation is supported by the electron and ion energy spectra shown in Fig. 8. In the case of a low-density target, both the hot electron temperature and ion energy decrease due to the radiation losses. As a whole there is essentially no difference in the high-density case.

V. CONCLUSIONS

The effect of radiation losses on the process of ion acceleration by ultraintense laser pulse is studied. It becomes important for laser intensities exceeding 10^{22} W/cm^2, where the radiation friction force slows down electrons and affects the ion dynamics through the self-consistent electrostatic field.

The effect of radiation losses depends strongly on the target density, thickness, and the laser polarization. It is less important in the case of strongly overdense targets and for a circular polarization, where the relative density n_e/n_c is larger than the laser amplitude, a_L. This is explained by clear spatial separation of the particles and fields. On the contrary, the radiation losses are important in the induced transparency regime where $n_e/n_c < a_L$. Although radiation losses are always leading to cooling of electrons, their effect on the ion distribution depends on the target thickness. In the case of thin targets, where the areal density is small, $\xi < a_L$, radiation losses may improve ion acceleration. In contrast, in the piston regime, $\xi > a_L$, radiation losses lead to a reduction of the piston velocity and less efficient ion acceleration.

Radiation losses of charged particles are incorporated in the electron dynamic equations by using the LAD models in Refs. [11,12,17,20]. The system of kinetic equations describing the radiation processes in the relativistic laser plasma interaction is presented and discussed. Both radiation models were implemented in the code PICLS and compared with previous publications. The radiation reaction force does not affect the numerical stability of the code and does not much penalize its performance.

The simulation results presented in this paper are limited to one spatial dimension. However, the particle momentum has three components, and arbitrary angles of electron propagation with respect to the laser wave are accounted for. We therefore do not expect any qualitative changes in two- or three-dimensional simulations. Recents results published in Ref. [30] confirm that statement. They demonstrated that results obtained for lower dimensionality remain valid qualitatively, although the maximum energy of ions in three dimensions is found to be higher than in corresponding simulations in one and two dimensions. We expect also that the magnetic fields generated in two- and three-dimensional simulations can be responsible for stronger radiation emission. Finally, extension of our model to regimes where $\chi_e \gtrsim 1$ can be done following the paper by Elkina *et al.* [22] where the electron-photon interaction and electron-positron pair production is described with the quantum cross sections.

ACKNOWLEDGMENTS

This work was partially supported in the European Union's Seventh Framework Programme, EURATOM within the "Keep-in-Touch" activities of the Marie Curie Project No. 230777. The authors are thankful to M. Grech for fruitful discussions and would like to thank Yasuhiko Sentoku for usage of the code PICLS.

[1] ELI project, http://www.extreme-light-infrastructure.eu/.
[2] S. V. Bulanov, Plasma Phys. Controlled Fusion **48**, B29 (2009).
[3] J. Fuchs *et al.*, Nat. Phys. **2**, 48 (2006); L. Robson *et al.*, *ibid.* **3**, 58 (2007).
[4] S. Wilks *et al.*, Phys. Plasmas **8**, 542 (2001); L. O. Silva, M. Marti, J. R. Davies, R. A. Fonseca, C. Ren, F. Tsung, and W. B. Mori, Phys. Rev. Lett. **92**, 015002 (2004); E. d'Humières, E. Lefebvre, L. Gremillet, and V. Malka, Phys. Plasmas **12**, 062704 (2005).
[5] S. V. Bulanov and V. S. Khoroshkov, Plasma Phys. Rep. **28**, 453 (2002); V. Malka *et al.*, Med. Phys. **31**, 1587 (2004).
[6] N. Naumova, T. Schlegel, V. T. Tikhonchuk, C. Labaune, I. V. Sokolov, and G. Mourou, Phys. Rev. Lett. **102**, 025002 (2009).
[7] T. Schlegel, N. Naumova, V. T. Tikhonchuk, C. Labaune, I. V. Sokolov, and G. Mourou, Phys. Plasmas **16**, 081303 (2009).
[8] P. A. M. Dirac, Proc. R. Soc. London A **167**, 148 (1938).
[9] F. V. Hartemann and A. K. Kerman, Phys. Rev. Lett. **76**, 624 (1996).
[10] J. Koga, T. Zh. Esirkepov, and S. V. Bulanov, Phys. Plasmas **12**, 093106 (2005).
[11] L. Landau and E. Lifschitz, *The Classical Theory of Fields*, 4th ed. (Pergamon, New York, 1994), Vol. 2.
[12] F. Rohrlich, *Classical Charged Particles*, 3rd ed. (World Scientific, Singapore, 2007).
[13] M. Tamburini, F. Pegoraro, A. Di Piazza, Ch. H. Keitel, and A. Macchi, New J. Phys. **12**, 123005 (2010).
[14] M. Chen, A. Pukhov, T.-P. Yu, and Z.-M. Sheng, Plasma Phys. Controlled Fusion **53**, 014004 (2011).
[15] A. R. Bell and J. G. Kirk, Phys. Rev. Lett. **101**, 200403 (2008).
[16] G. W. Ford and R. F. O'Connell, Phys. Lett. A **174**, 182 (1993).

[17] I. V. Sokolov, J. Exp. Theor. Phys. **109**, 207 (2009).
[18] I. V. Sokolov, N. M. Naumova, J. A. Nees, G. A. Mourou, and V. P. Yanovsky, Phys. Plasmas **16**, 093115 (2009).
[19] I. V. Sokolov, J. A. Nees, V. P. Yanovsky, N. M. Naumova, and G. A. Mourou, Phys. Rev. E **81**, 036412 (2010).
[20] I. V. Sokolov, N. M. Naumova, and J. A. Nees, Phys. Plasmas **18**, 093109 (2011).
[21] Y. Sentoku and A. Kemp, J. Comput. Phys. **227**, 6846 (2008).
[22] N. V. Elkina, A. M. Fedotov, I. Yu. Kostyukov, M. V. Legkov, N. B. Narozhny, E. N. Nerush, and H. Ruhl, Phys. Rev. ST Accel. Beams **14**, 054401 (2011).
[23] M. Tamburini, F. Pegoraro, A. Di. Piazza, Ch. H. Keitel, T. V. Liseykina, and A. Macchi, Nucl. Inst. Meth. A **653**, 181 (2011).
[24] C. K. Birdsall and A. B. Langdon, *Plasma Physics via Computer Simulation* (IoP Publishing, Bristol, 2005).
[25] M. Grech, S. Skupin, R. Nuter, L. Gremillet, and E. Lefebvre, New J. Phys. **11**, 093035 (2009).
[26] M. Grech, S. Skupin, R. Nuter, L. Gremillet, and E. Lefebvre, Nucl. Inst. Meth. A **620**, 63 (2010).
[27] V. A. Vshivkov, N. M. Naumova, F. Pegoraro, and S. V. Bulanov, Phys. Plasmas **5**, 2727 (1998).
[28] A. Macchi, S. Veghini, and F. Pegoraro, Phys. Rev. Lett. **103**, 085003 (2009).
[29] T. V. Liseykina, M. Borghesi, A. Macchi, and S. Tuveri, Plasma Phys. Controlled Fusion **50**, 124033 (2008).
[30] M. Tamburini, T. V. Liseykina, F. Pegoraro, and A. Macchi, Phys. Rev. E **85**, 016407 (2012).